The *M*-Integral Analysis for a Nano-Inclusion in Plane Elastic Materials Under Uni-Axial or Bi-Axial Loadings

Tong Hui

Yi-Heng Chen
e-mail: yhchen2@mail.xjtu.edu.cn

School of Aerospace,
SVL,
Xi'an Jiaotong University,
28 Xianning West Road,
Xi'an, Shaanxi, 710049, P.R.China

*This paper deals with the M-integral analysis for a nano-inclusion in plane elastic materials under uni-axial or bi-axial loadings. Based on previous works (Gurtin and Murdoch, 1975, "A Continuum Theory of Elastic Material Surfaces," Arch. Ration. Mech. Anal., **57**, pp. 291–323; Mogilevskaya, et al., 2008, "Multiple Interacting Circular Nano-Inhomogeneities With Surface/Interface Effects," J. Mech. Phys. Solids, **56**, pp. 2298–2327), the surface effect induced from the surface tension and the surface Lamé constants is taken into account, and an analytical solution is obtained. Four kinds of inclusions including soft inclusion, hard inclusion, void, and rigid inclusions are considered. The variable tendencies of the M-integral for each of four nano-inclusions against the loading or against the inclusion radius are plotted and discussed in detail. It is found that in nanoscale the surface parameters for the hard inclusion or rigid inclusion have a little or little influence on the M-integral, and the values of the M-integral are always negative as they would be in macroscale, whereas the surface parameters for the soft inclusion or void yield significant influence on the M-integral and the values of the M-integral could be either positive or negative depending on the loading levels and the surface parameters. Of great interest is that there is a neutral loading point for the soft inclusion or void, at which the M-integral transforms from a negative value to a positive value, and that the bi-axial loading yields similar variable tendencies of the M-integral as those under the uni-axial tension loading. Moreover, the bi-axial tension loading increases the neutral loading point, whereas the bi-axial tension-compression loading decreases it. Particularly, the magnitude of the negative M-integral representing the energy absorbing of the soft inclusion or void increases very sharply as the radius of the soft inclusion or void decreases from 5 nm to 1 nm.* [DOI: 10.1115/1.3176997]

Keywords: M-integral, nano-inclusion, Gurtin and Murdoch model, surface tension, surface Lamé constants

1 Introduction

The microelectomechanical system (MEMS) and advanced materials in the nanometer scale become increasingly popular owing to their widely potential applications in constructing new microinstruments and highly effective memory materials. Common examples are nanowires, nanotubes, nanoplates, etc., which motivate a new interest in nanomechanics. A detailed review has been given by Ortiz [1]. In addition, materials with nano-inclusions/tubes as reinforcing elements represent disparate mechanical, electronic, and optical properties due to influence conducted by the nanoscale surface/interface. Accordingly, it is hard-pressed to study material properties in nanoscale for the further development of nanotechnology [2,3].

Size dependency of effective properties and elastic field of nanoscale elements can be explained by accounting for the effect of surface stresses that are associated with the excess free energy of a surface. In classical mechanics in macroscale, the bulk elastic energy controls the behavior of a material element, whereas for nanosized structure the influence of surface effect becomes significant due to the comparatively high surface/volume ratio of nanosized inclusion/void. Furthermore, tests on some elementary deformation modes such as uni-axial stretching plates, bending of beams, and torsion of bars manifest that the surface elasticity agree well with directly atomic simulations [4,5]. Accordingly, it is rational to employ the elastic continuum theory to account for the influence of the surface/interface effect in nanoscale.

On the one hand, the roots of surface energy lie in the thermodynamics of solid surfaces as formulated by Gibbs [6]. Using this formulation, Nix and Gao [7] proposed an atomistic interpretation of interface stress, in which an explicit relationship between surface/interface stress and strain was given in the Eulerian coordinate system. Besides, Gurtin and Murdoch [8] and Gurtin et al. [9] presented a continuum mechanics theory to account for the surface energy or interface energy. In the recent years, much attention is focused on the investigations of material properties in nanoscale by using the elastic continuum theory. The influence of surface effect on the solution of an isolated spherical or cylindrical inclusion embedded in an infinite or semifinite matrix was investigated by Sharma and co-workers [10–13], Duan and coworkers [14,15], Lim et al. [16], Tian and Rajapakse [17], and Mogilevsaya et al. [18], among many others. Besides, some material properties are also considered such as the surface effects on the diffraction of plane compressional waves by a nanosized circular hole [17], the effective moduli of solids with nano-inclusions [19,20], the nanovoid deformation in aluminum under simple shear [21], and the conservational integrals with consideration of surface effect influence [22]. Now, there are a number of publications concerned with the stress analyses of nano-inclusions

Contributed by the Applied Mechanics Division of ASME for publication in the JOURNAL OF APPLIED MECHANICS. Manuscript received December 13, 2008; final manuscript received June 1, 2009; published online December 14, 2009. Review conducted by Yonggang Huang.

or the effective properties and elastic field of nanofiber reinforced composites (see, e.g., Refs. [23–35], among many others).

On the other hand, the well-known conservation integrals derived from Noether's theorem in plane elasticity including the J_k-integral vector, M-integral, and L-integral [36–41] were established in classical fracture mechanics. With the presence of a defect, evaluations of the above tour integrals along a counterclockwise contour enclosing the defect result in the so-called driving forces in moving, expansion, and rotation of the defect, respectively. Thus, the J-integral, as the first component of the J_k-vector, has much less significance than the M-integral and the L-integral when the closed contour surrounds the defect completely [40]. Although the applications of the M-integral and L-integral are not as common as the J-integral, they did have some physical significance when the integration contour surrounds a single defect or macrodefects completely [41–45]. This implies their application in fracture mechanics for multidefects in materials and structures, provided that the integration contour is suitably chosen, i.e., it surrounds all defects completely. For example, the M-integral was used to describe the energy release due to a cloud of the macrodefects in the work of Chen [44,45] where the M-integral has been proved to be an effective parameter in describing the configuration change in the many defects. Besides, the M-integral applied in the nanovoided material was investigated by Li and Chen [46]. Nonetheless, their work was only limited in the case of a nanovoid under uni-axial tensile loadings. Moreover, they have not found the negative values of the M-integral representing the energy absorbing due to the nanovoid expansion. It seems that the M-integral analyses for different kinds of nano-inclusion, e.g., soft or hard inclusion. etc., under bi-axial tension loading or under bi-axial tension-compression loading are worthy of further studying, from which the physical features of the M-integral in nanoscale could be clarified in more details.

The goal of this paper is to provide the lack of the understanding of the role played by the M-integral in different kinds of nano-inclusions under three kinds of loadings: the uni-axial tension loading, the bi-axial tension loading, and the bi-axial tension-compression loading. This paper is organized as follows. In Sec. 2, the basic formulations are presented and an analytical solution of the deformation field for an infinite elastic plane containing a nano-inclusion as influenced by the surface effect is obtained. In Sec. 3, the analytical expressions and some basic properties of the M-integral and the J_k-integral vector are presented in nanoscale. Numerical results are shown in figures, and the variable tendencies of the M integral against the loading levels or against the inclusion radius are discussed in Sec. 4. In Sec. 5, some conclusions and remarks are summarized.

2 Elastic Field of a Circular Inclusion

The size dependency of surface effect that is related to the excess free energy of a surface could be explained by accounting for the surface stress tensors. The conditions imposed at the material surface yield the surface tension and surface elasticity, which are substantially used to solve the problems involving a nano-inclusion as shown in Fig. 1. Accordingly, the presence of surface/interface stress should be accounted for in the present work. Applying the model of Gurtin and Murdoch [8] who gave equations that describe the conditions at the surface with consideration of the surface energy effect yields the following equations:

$$\mathbf{u}^{\text{int}} = \mathbf{u}^{\text{mat}} = \mathbf{u} \quad \text{(continuity of the displacements)} \tag{1}$$

$$(\boldsymbol{\sigma}^{\text{int}} - \boldsymbol{\sigma}^{\text{mat}})\mathbf{n} = \text{div}_{\Sigma}\mathbf{S} \quad \text{(equilibrium of the interface)} \tag{2}$$

$$\mathbf{S} = \sigma_0\mathbf{I}_l + (\lambda_0 + \sigma_0)(\text{tr}\,\boldsymbol{\varepsilon}^{\text{sur}})\mathbf{I}_l + 2(\mu_0 - \sigma_0)\boldsymbol{\varepsilon}^{\text{sur}} + \sigma_0\nabla_{\Sigma}\mathbf{u} \quad \text{(surface constitutive equations)} \tag{3}$$

where the superscripts "int" and "mat" denote the nano-inclusion and the matrix, respectively; $\mathbf{n}$ represents a unit normal vector to the surface that points away from the inclusion; $\boldsymbol{\sigma}$ is the stress tensor of the bulk material; $\mathbf{S}$ is the (first) Piola–Kirchhoff surface stress tensor; div_{Σ} is the surface divergence in its original configuration Σ (before the deformation caused by the external loading); σ_0 is the surface tension; λ_0 and μ_0 are the surface Lamé constants; $\mathbf{I}_l$ stands for the unit tangent tensor; and tr $\boldsymbol{\varepsilon}^{\text{sur}}$ is the trace of the surface strain tensor $\boldsymbol{\varepsilon}^{\text{sur}}$; and ∇_{Σ} is the surface gradient of the displacement field.

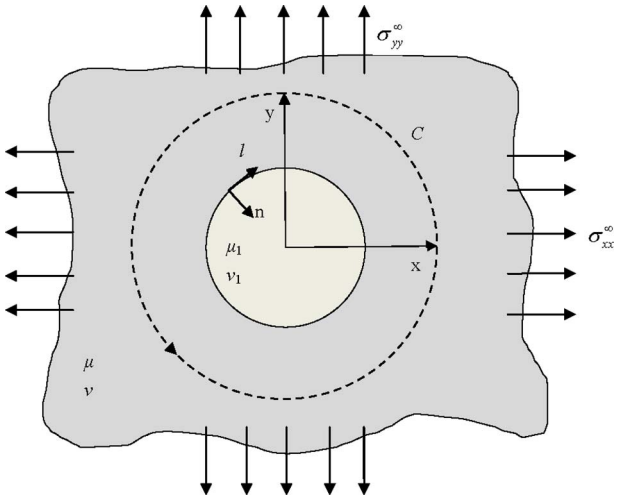

Fig. 1 Local-global coordinate systems for the two-dimensional problem with a circular nano-inclusion under bi-axial loadings

Using the foregoing Eqs. (1)–(3), Mogilevskaya et al. [18] obtained the governing functions for the deformation field for the two-dimensional isotopic elastic problem containing multi-interacting nano-inhomogeneities. According to their work, the generic equations for the plane strain state become the following:

$$u^{\text{int}}_{kx} = u^{\text{mat}}_{kx} = u_{kx}, \quad u^{\text{int}}_{ky} = u^{\text{mat}}_{ky} = u_{ky} \quad \text{(continuity of the displacements)} \tag{4}$$

$$\sigma^{\text{int}}_{kl} - \sigma^{\text{mat}}_{kl} = \frac{\partial \sigma^{\text{sur}}_k}{\partial s} + \frac{\sigma_{k0}\omega^{\text{sur}}_k}{R_k}, \quad \text{(Equilibrium of the interface)} \tag{5}$$

$$\sigma^{\text{int}}_{kn} - \sigma^{\text{mat}}_{kn} = -\frac{1}{R_k}\sigma^{\text{sur}}_k + \frac{\sigma_{k0}\,\partial\,\omega^{\text{sur}}_k}{\partial s}, \tag{6}$$

$$\sigma^{\text{sur}}_k = \sigma_{k0} + (2\mu_{k0} + \lambda_{k0})\varepsilon^{\text{sur}}_k. \quad \text{(Surface constitutive equations)} \tag{7}$$

where u_{kx} and u_{ky} are the components of the displacement vector $\mathbf{u}_k$ on the boundary $L_k(k=1,2,\ldots,N)$; s is the arc length of a boundary; σ_{kl}, σ_{kn}, and σ^{sur}_k for the kth sub-boundary; L_k are the normal traction, the shear traction, and the surface stress component; $\varepsilon^{\text{sur}}_k$ is the one-dimensional strain component. Particularly, the local coordinate system for the foregoing generic equations is chosen in such a way that the normal $\mathbf{n}$ points away from the inclusion and the tangent direction $\boldsymbol{l}$ is traveling leaving the inclusion on the left (see Fig. 1).

In the present work, attention will be focused on the M-integral analysis and the investigation will be limited to the case of a circular inclusion characterized by its radius R as shown in Fig. 1, where the tractions on the matrix and the stress functions in the matrix read as follows [18]:

$$\sigma^{\text{mat}}(\tau) = B^{\text{mat}}_{-21}g^2(\tau) + B^{\text{mat}}_{01} + B^{\text{mat}}_{21}g^{-2}(\tau) \tag{8}$$

and

$$\varphi = \frac{2}{\kappa+1}[-(\mu_1-\mu+\eta_1^{(1)})A_{-11}g(z)+3\eta_1^{(2)}\bar{A}_{31}g(z)]+\varphi^{\infty}(z)$$

$$\psi(z) = \frac{1}{\kappa+1}\left\{4\left[\left(\mu_1\frac{\kappa-1}{\kappa_1-1}-\mu+(\kappa-1)\eta_1\right)\mathrm{Re}\,A_{11}+\frac{\kappa-1}{4}\sigma_0\right]g(z)+2\left[\left(\frac{\bar{z}}{R}+g(z)\right)(\mu-\mu_1-\eta_1^{(1)})-\kappa\eta_1^{(2)}g(z)\right]A_{-11}g^2(z)+2\left[3\eta_1^{(2)}\left(\frac{\bar{z}}{R}+g(z)\right)+g(z)\left(\mu_1\frac{\kappa}{\kappa_1}-\mu+3\kappa\eta_1^{(1)}\right)\right]\bar{A}_{31}g^2(z)\right\}+\psi^{\infty}(z) \tag{9}$$

with

$$\varphi^{\infty}(z) = \frac{(\sigma_{xx}^{\infty}+\sigma_{yy}^{\infty})}{4}z$$

$$\psi^{\infty}(z) = \frac{(\sigma_{yy}^{\infty}-\sigma_{xx}^{\infty}+2\mathrm{i}\sigma_{xy}^{\infty})}{2}z \tag{10}$$

where $z=x+iy$ is the complex coordinate of a point (x,y) in the matrix, σ_{xx}^{∞}, σ_{yy}^{∞}, and σ_{xy}^{∞} are external stresses at infinity, z_0 refers to the center point of the circular inclusion, and τ is a point on the interface, $\kappa=3-4\nu$ for plane strain problem, where ν is Poisson's ratio of the matrix material, and $\kappa_1=3-4\nu_1$ refers to the inclusion.

In Eq. (8), $\sigma^{\mathrm{mat}}(\tau)$ is a complex function, which could be expressed by $\sigma^{\mathrm{mat}}(\tau)=\sigma_n^{\mathrm{mat}}(\tau)+i\sigma_l^{\mathrm{mat}}(\tau)$ in the local coordinate system as defined in Fig. 1. Besides, the function $g(z)$ and the coefficients **B** read the following formulations:

$$g(z) = \frac{R}{z-z_0} \tag{11}$$

and

$$B_{01}^{\mathrm{mat}} = \frac{\mu}{2R\Delta_1}\sigma_0+\frac{\kappa+1}{4}\frac{\mu_1+\eta_1(\kappa_1-1)}{\Delta_1(\kappa_1-1)}(\sigma_{xx}^{\infty}+\sigma_{yy}^{\infty})$$

$$B_{-21}^{\mathrm{mat}} = -\frac{\kappa+1}{2}\frac{(\mu_1+\eta_1^{(1)})(\mu\kappa_1+\mu_1)+3\mu_1\kappa_1\eta_1^{(1)}+3\kappa_1\eta_1\sigma_0/R}{\Delta_2}\times(\sigma_{yy}^{\infty}-\sigma_{xx}^{\infty}-2\mathrm{i}\sigma_{xy}^{\infty}) \tag{12}$$

$$B_{21}^{\mathrm{mat}} = 3\frac{\kappa+1}{2}\frac{\mu\kappa_1\eta_1^{(2)}}{\Delta_2}(\sigma_{yy}^{\infty}-\sigma_{xx}^{\infty}+2\mathrm{i}\sigma_{xy}^{\infty})$$

in which

$$\Delta_1 = \frac{\mu_1}{\kappa_1-1}+\frac{\mu}{2}+\eta_1 \tag{13}$$

$$\Delta_2 = (\kappa\mu_1+\mu)(\mu\kappa_1+\mu_1)+\eta_1^{(1)}[3\kappa_1(\kappa\mu_1+\mu)+\kappa(\mu\kappa_1+\mu_1)]+3\kappa\kappa_1\eta_1\frac{\sigma_0}{R},$$

and

$$\eta_1 = (2\mu_0+\lambda_0)/(4R), \quad \eta_1^{(1)} = \eta_1+0.25\sigma_0/R, \quad \eta_1^{(2)} = \eta_1-0.25\sigma_0/R \tag{14}$$

In Eq. (9), the complex coefficients A is given as follows

$$\mathrm{Re}\,A_{11} = -\frac{1}{4\Delta_1}\sigma_0+\frac{\kappa+1}{4}\frac{1}{4\Delta_1}R(\sigma_{xx}^{\infty}+\sigma_{yy}^{\infty})$$

$$A_{-11} = -\frac{\kappa+1}{4}\frac{\mu\kappa_1+\mu_1+3\kappa_1\eta_1^{(1)}}{\Delta_2}R(\sigma_{yy}^{\infty}-\sigma_{xx}^{\infty}-2\mathrm{i}\sigma_{xy}^{\infty}) \tag{15}$$

$$A_{31} = -\frac{\kappa+1}{4}\frac{\kappa_1\eta_1^{(2)}}{\Delta_2}R(\sigma_{yy}^{\infty}-\sigma_{xx}^{\infty}+2\mathrm{i}\sigma_{xy}^{\infty})$$

Particularly, it should be emphasized that the present manipulation is derived directly from the model of Gurtin and Murdoch [8] accounting for the surface tension and surface Lamé constants without any simplification [18]. Thus, the foregoing stress functions could be used to represent the complete relation between the M-integral and the surface effect for different kinds of inclusions in nanoscale.

3 Basic Formulas and Properties of the M-Integral and J_k-Integral in Nanoscale

The M-integral and the J_k-integral vector in macro-elasticity are formulated as follows [36–41]:

$$M = \oint_C (wx_ie_i - T_ku_{k,i}x_i)ds \tag{16}$$

$$J_k = \oint_C (we_k - u_{i,k}T_i)ds \quad (k=1,2) \tag{17}$$

where C is a counterclockwise contour, which enclosed the whole nanosized inclusion as shown in Fig. 1; $w=s_{ij}\varepsilon_{ij}/2$ denotes the strain energy density; and T_k is the traction acting on the outside of a closed contour C, x_j with $j=1,2$ represents a rectangular plane coordinate system, e_i refers to the outside normal component of the contour C and s is the arc length of the contour C.

It is noticed from Fig. 1 that the only difference in performing the M-integral analysis for a nano-inclusion from those for a macro/micro-inclusion is the role played by the surface/interface effect. It is well-known in classical defect mechanics that the surface of a macro/micro-void is traction-free, whereas the surface energy effect for a nanovoid should be accounted for, although the path-independent feature of the invariant integrals remains unchanged. For convenience, it is useful to translate the expressions of such invariant integrals to the polar coordinate system (ρ,θ) as shown in Fig. 1, which are given below.

$$J_1 = \oint_C \left\{w\cos\theta-\left(\varepsilon_{\rho\rho}\cos\theta-\frac{\sin\theta}{\rho}\frac{\partial u_\rho}{\partial\theta}\right)T_\rho-\left(\frac{\partial u_\theta}{\partial\rho}\cos\theta-\frac{\sin\theta}{\rho}\frac{\partial u_\theta}{\partial\theta}\right)T_\theta\right\}ds \tag{18}$$

$$J_2 = \oint_C \left\{w\sin\theta-\left(\varepsilon_{\rho\rho}\sin\theta+\frac{\cos\theta}{\rho}\frac{\partial u_\rho}{\partial\theta}\right)T_\rho-\left(\frac{\partial u_\theta}{\partial\rho}\sin\theta+\frac{\cos\theta}{\rho}\frac{\partial u_\theta}{\partial\theta}\right)T_\theta\right\}ds \tag{19}$$

$$M = \oint_C \left[w-T_\rho\varepsilon_{\rho\rho}-T_\theta\left(2\varepsilon_{\rho\theta}+\frac{u_\theta}{\rho}-\frac{1}{\rho}\frac{\partial u_\theta}{\partial\theta}\right)\right]\rho ds \tag{20}$$

On the one hand, according to the intrinsic path-independence of the invariant integrals, a special circular contour in Eqs. (18)–(20) is adopted as the closed integral path (see the contour C in Fig. 1), along which the following expressions are given:

$$T_\rho = \sigma_{\rho\rho}, \quad T_\theta = \sigma_{\rho\theta}, \quad ds = \rho d\theta \tag{21}$$

which bring some significant convenience in the forthcoming calculations.

On the other hand, the independence of the M-integral from the coordinate system shift or rotation should also be clarified in nanoscale when taking the surface effect into account. When the coordinate axes (x_1, x_2) are rotated by an angle φ^*, a new coordinate system (x_1^*, x_2^*) is proposed. Since the M-integral is an inner product of the J_k-integral vector and the vector $x_k = (x_1, x_2)$, as defined in Eq. (16), it is scalar and then the invariant feature after the rotation yields

$$M^*(x_1^*, x_2^*) = M(x_1, x_2) \tag{22}$$

where the integrals $M^*(x_1^*, x_2^*)$ and $M(x_1, x_2)$ are defined in the system (x_1^*, x_2^*) and (x_1, x_2), respectively.

In addition, whether the M-integral varies when the rectangular coordinate system (x_1, x_2) shifts to another one (x_{01}, x_{02}) should be clarified by the following relations:

$$\begin{aligned} x_1 &= x_{01} - \xi_1 \\ x_2 &= x_{02} - \xi_2 \end{aligned} \tag{23}$$

where (ξ_1, ξ_2) denote the shifts of the new rectangular coordinate system (x_{01}, x_{02}) from the original system (x_1, x_2).

The value of the M-integral in the new system (x_{01}, x_{02}) denoted by M' could be given by substituting Eq. (23) into Eq. (16). Thus, it follows that

$$M'(x_{01}, x_{02}) = \oint_C (w x_{0i} e_i - T_k u_{k,i} x_{0i}) ds = M(x_1, x_2) + \xi_1 J_1(x_1, x_2) + \xi_2 J_2(x_1, x_2) \tag{24}$$

Obviously, the first term on the right hand side of Eq. (24) is just the same as the M-integral in the original system (x_1, x_2), whereas the second and the third terms on the right hand side of Eq. (24) involve the two components of the J_k-integrals. Fortunately, these two components do vanish in the present case as they would do in macro-/microscale [44]. This is because the stresses induced from the surface effect have a $1/r^2$ asymptote feature as $r \to \infty$ [44,45]. Thus, the M-integral could be either independent from the coordinate shifts or from the coordinate rotation in the present problem with a nanoscale inclusion.

Actually, the displacements and stresses for the present problem shown in Fig. 1 can be evaluated by using the complex potentials as follows:

$$\begin{aligned} \sigma_{xx} + \sigma_{yy} &= 4 \,\mathrm{Re}\, \varphi'(z) \\ \sigma_{yy} - \sigma_{xx} + 2\mathrm{i}\sigma_{xy} &= 2[\bar{z}\varphi''(z) + \psi'(z)] \\ 2\mu(u_x(z) + \mathrm{i}u_y(z)) &= \kappa\varphi(z) - z\overline{\varphi'(z)} - \overline{\psi(z)} \end{aligned} \tag{25}$$

By substituting Eq. (9) into Eq. (25), the complete stress and displacement field could be obtained without any difficulty. After using Eqs. (18)–(20) and making some lengthy and straightforward manipulations, the explicit formulations of the three invariant integrals have the following forms:

$$\begin{aligned} J_1 &= 0 \\ J_2 &= 0 \end{aligned} \tag{26}$$

$$M = \frac{\pi R(1+\kappa)[2\ \mathrm{Co}\ 1(\sigma_{xx}^\infty - \sigma_{yy}^\infty) - \mathrm{Co}\ 2(\sigma_{xx}^\infty + \sigma_{yy}^\infty)]}{4\mu} \tag{27}$$

where

$$\mathrm{Co}\ 1 = \frac{2}{\kappa+1}[-(\mu_1 - \mu + \eta_1^{(1)})A_{-11} + 3\eta_1^{(2)}A_{31}] \tag{28}$$

$$\mathrm{Co}\ 2 = \frac{1}{\kappa+1}\left\{4\left[\left(\mu_1\frac{\kappa-1}{\kappa_1-1} - \mu + (\kappa-1)\eta_1\right)A_{11} + \frac{\kappa-1}{4}\sigma_0\right]\right\}$$

with $\eta_1 = (2\mu_0 + \lambda_0)/(4R)$, $\eta_1^{(1)} = \eta_1 + 0.25\sigma_0/R$, $\eta_1^{(2)} = \eta_1 - 0.25\sigma_0/R$ defined in Eq. (14).

In the manipulation of Eq. (27), it has been assumed that there is no shear loading at infinity, i.e., $\sigma_{xy}^\infty = 0$. Moreover, the following identities have been used:

$$\int_0^{2\pi} \cos(n\theta) d\theta = 0, \quad \int_0^{2\pi} \sin(n\theta) d\theta = 0 \quad (n \neq 0) \tag{29}$$

From Eq. (26), it is clearly shown that the J-integral (J_1) vanishes, which has no physical significance in the present problem, whereas the M-integral does not vanish, in general, which is independent from the coordinate shifts, although the M-integral is nowhere near as prevalent in the mechanics literature as the J-integral. This is very important for the subsequent discussions because these identities could enhance the convenience of measuring the M-integral and pave a way for wide application of the M-integral by establishing the relation between the M-integral and the surface energy effect as investigated in detail in Sec. 4. Hereto, the analytical expression of the M-integral has been given in Eq. (27) with Eqs. (28) and (14) accounting for the surface energy effect. Evaluating expression (27) for different kinds of nano-inclusions subjected to different kinds of loading will facilitate better understanding and will provide the main features of the surface energy effect on the M-integral in nanoscale.

4 Influence of the Different Kinds of Inclusion on the M-Integral in Nanoscale

In this section, the influence induced from each of the four different kinds of nano-inclusion on the M-integral is discussed. The different kinds of nano-inclusion, the different radiuses of inclusion, the different surface parameters along the inclusion surface, and the different kinds of loadings are considered and discussed in detail. Unlike the work of Li and Chen [46] who only discussed in detail the influence of the surface parameters to the M-integral for a nanohole under the simple uni-axial tensile loading, this section deals with the four kinds of defect: void, soft inclusion, hard inclusion, and rigid inclusion under three different kinds of loading conditions: the uni-axial tensile loading, the bi-axial tensile loadings, and the bi-axial tension-compression loadings, respectively. In the engineering practice such as the nanowire, nanofiber, etc., the investigation of nano-inclusion (hard or nearly rigid) seems to be more useful. Moreover, in the previous work [46] with respect to the deformation field induced from the nano-inclusion or void, the model of Gurtin and Murdoch [8] was simplified. This disposal might omit some important features when applying the M-integral concept to describe the nanoscale defect problems. Accordingly, the present stress and displacement fields, which are derived directly from the complete model of Gurtin and Murdoch without any simplification, will facilitate the better understanding of the influence of each of the four kinds of nano-inclusion on the M-integral.

In order to make detailed comparisons, in the following discussions, three kinds of loading conditions are considered: (a) the uni-axial tension loading, $\sigma_{yy}^\infty = p$; (b) the bi-axial tension loading, $\sigma_{xx}^\infty = \sigma_{yy}^\infty = p$, and (c) a bi-axial tension-compression loading with $\sigma_{yy}^\infty = p$ and $\sigma_{xx}^\infty = -p/2$, respectively. Moreover, four different kinds of nano-inclusion are individually discussed: (A) the *soft inclusion* with $\mu 1 = 0.5\mu$, $\nu 1 = \nu$; (B) the *rigid inclusion* with $\mu 1 \to \infty$, $\nu 1 = \nu$; (C) the *void* with $\mu 1 = 0$, $\nu 1 = 0$; and (D) the *hard*

inclusion with $\mu 1 = 3\mu$, $\nu 1 = \nu$, respectively. In addition, by following the work [16], two sets of surface parameters are employed: (i) $\mu_0 = -5.4251$ N/m, $\lambda_0 = 3.4939$ N/m, and $\sigma_0 = 0.5689$ N/m for Al [1 0 0] surface; (ii) $\mu_0 = -0.3760$ N/m, $\lambda_0 = 6.8511$ N/m, and $\sigma_0 = 0.9108$ N/m for Al[1,1,1] surface. Although the surface properties are generally anisotropic, it is assumed that the isotropic case is sufficient to illustrate the main features of the size-dependent response as Tian and Rajapakse did in Ref. [17].

First, the influence of the four different kinds of inclusion on the M-integral under the three different kinds of loading is considered by setting the radius of the inclusions to be a constant, say, 5 nm. Here, throughout this paper, the matrix material is always taken to be $\mu = 34.7$ GPa and $\nu = 0.331$. For the four different kinds of inclusion with the radius $R = 5$ nm, numerical results are shown in Figs. 2(*a*)–2(*c*) and 3(*a*)–3(*c*), corresponding to (i) those of the first set of surface parameters and (ii) those of the second set of surface parameters, respectively [17]. It should be mentioned that Fig. 2(*a*) or Fig. 3(*a*) corresponds to those under the uni-axial tension loading, Fig. 2(*b*) or Fig. 3(*b*) corresponds to those under the uniform bi-axial tension loading with $\sigma_{xx}^{\infty} = \sigma_{yy}^{\infty} = p$, whereas Fig. 2(*c*) or Fig. 3(*c*) corresponds to those under the bi-axial tension-compression loading with $\sigma_{yy}^{\infty} = p$ and $\sigma_{xx}^{\infty} = -p/2$.

It is found from Fig. 2(*a*) that the variable curves for the two kinds of inclusion: (B) the rigid inclusion with symbol (●) and (D) the hard inclusion with symbol (▼) as mentioned above always yield negative values of the M-integral no matter how large the uni-axial tension loading is. This is not a surprise because the M-integral represents the energy release due to the defect expansion [36–40], whereas the expansion of a rigid inclusion or a hard inclusion always yields the negative energy release, i.e., the energy absorbing. In other words, the size effect of the rigid or hard inclusion could only change the magnitude of the M-integral but could not change the negative feature of the M-integral, i.e., the energy absorbing due to the inclusion expansion. The larger the uni-axial tension loading is, the larger the absolute value of the negative M-integral is, as it would be in macro-/microscale. Nevertheless, for the homogeneous case, i.e., the materials of inclusion and the matrix are the same without interface, it is obvious that the M-integral should vanish. However, the other two cases: (A) the soft inclusion and (C) the void as mentioned above should be studied in more details. Figure 2(*a*) reveals that the variable curves for the soft inclusion with symbol (□) and the void with symbol (△) may yield either negative or positive values of the M-integral, depending on the uni-axial tension loading level. In other words, the expansion of a nanosoft inclusion or a nanovoid may either release the energy or absorb the energy, depending on the loading level. This feature has not been found by Li and Chen [46]. For example, in Fig. 2(*a*), when the tension loading is less than about 70 MPa for the case (C), i.e., a nanovoid of 5 nm, and about 90 MPa for the case (A), i.e., the soft inclusion of 5 nm, the values of the M-integral are always negative (i.e., absorbing energy), whereas when the tension loading increases over 70 MPa or 90 MPa for the two kinds of inclusion (A) or (C), respectively, the nanovoid or the nanosoft inclusion will yield positive values of the M-integral (i.e., release energy). In the latter case, the larger the uni-axial tension loading is, the larger the positive M-integral is. Of great interest is that there is a special loading level called the neutral loading point, at which the M-integral transformation from a negative value to a positive value occurs. However, the other two kinds of inclusion (B) and (D) show quite different features from the cases (A) and (C) as seen in Fig. 2(*a*), in which the larger the uni-axial tension loading is, the larger of the absolute values of the negative M-integral is without the neutral loading point. Moreover, the slopes of the variable curves of the two kinds of inclusion (B) and (D) are quite different. It is seen from Fig. 2(*a*) that the rigid inclusion always yields larger influence on the negative values of the M-integral than the hard inclusion. As regards to Fig. 2(*b*) under the uniform bi-axial tension loading, it

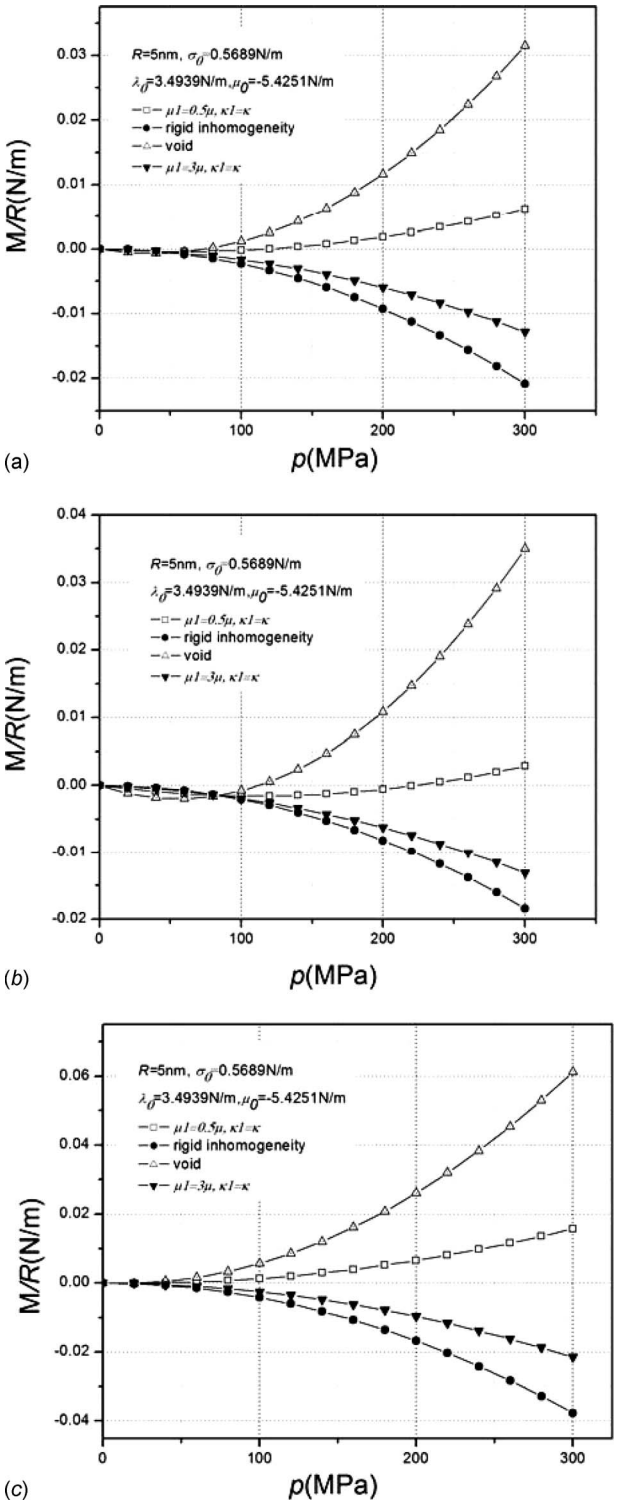

Fig. 2 The influence of different kinds of inclusion on the *M*-integral: (*a*) uni-axial tension loading, (*b*) bi-axial tension loading, and (*c*) bi-axial tension-compression loading

is seen that the variable tendencies of the four curves are similar to those shown in Fig. 2(*a*). The only differences are the values of the neutral loading point for the cases (A) and (C). In Fig. 2(*b*) the neutral loading points are 115 MPa and 220 MPa corresponding to the void and the soft inclusion, respectively, much larger than those under the uni-axial tension loading. This means that the uniform bi-axial tension loading yields much smaller influence of

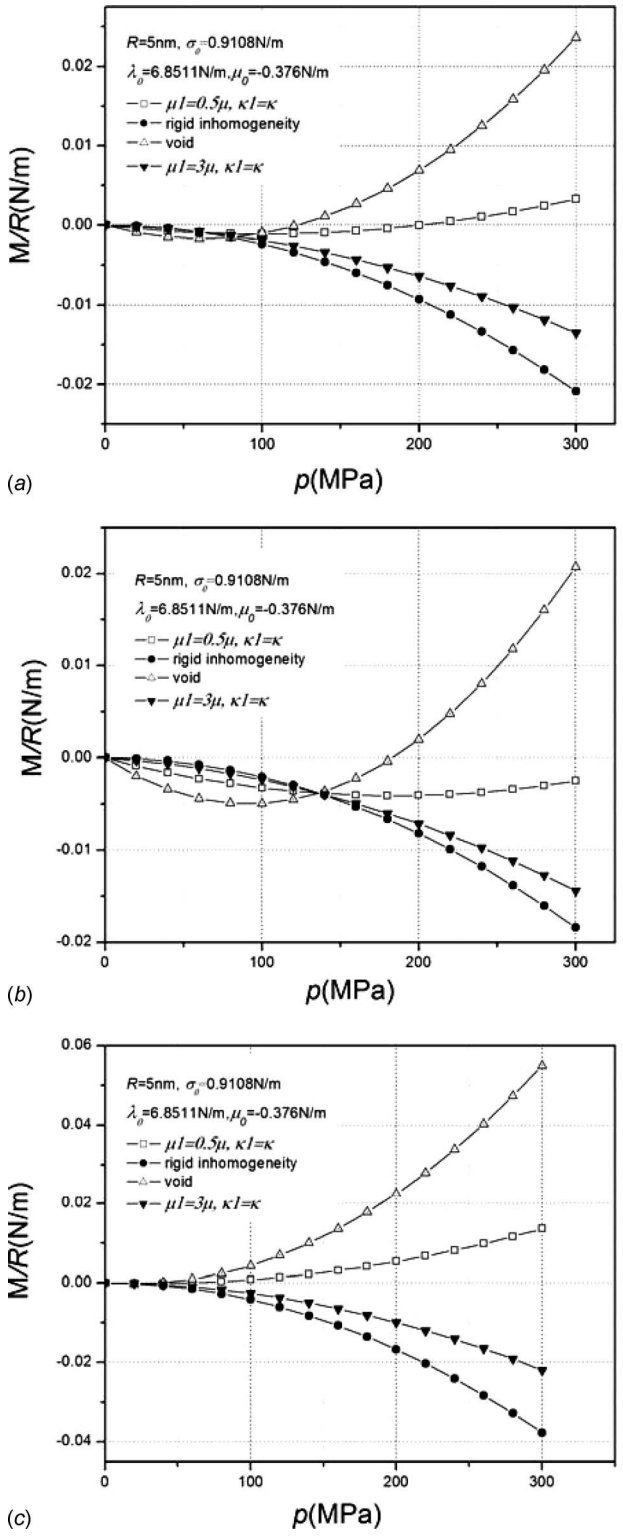

Fig. 3 The influence of different kinds of inclusion on the *M*-integral: (*a*) uni-axial tension loading, (*b*) bi-axial tension loading, and (*c*) bi-axial tension-compression loading

the M-integral, e.g., it increases the neutral loading point significantly but the variable tendencies are not changed as compared with those under the uni-axial loading. Of great interest is the variable tendencies shown in Fig. 2(c) for the bi-axial tension-compression loading with $\sigma_{yy}^{\infty}=p$ and $\sigma_{xx}^{\infty}=-p/2$, where the values of the neutral loading point for the void or the soft inclusion are merely 24 MPa and 35 MPa, respectively, much smaller than those under the uni-axial tension loading. That is, in the most cases under consideration when $p>24$ MPa or $p>35$ MPa, the values of the M-integral for the void or for the soft inclusion are always positive. In other words, the expansion of the void or the soft inclusion under this loading level always releases energy. This demonstrates that the horizontal compression loading will yield a significant influence on the M-integral for the void and the soft inclusion. Moreover, it is seen from a detailed comparison among Figs. 2(a)–2(c) that the horizontal compression loading significantly increases the magnitude of the M-integral under $p=300$ MPa. For example, under $p=300$ Mpa, the values of the M-integral divided by $R=5$ nm are 0.032, 0.035, and 0.06 for the void in Figs. 2(a)–2(c), respectively, and the latter is much larger than the two formers; whereas the values of the M-integral divided by $R=5$ nm are -0.021, -0.019, and -0.038 for the rigid inclusion in Figs. 2(a)–2(c), respectively, and the magnitude of the latter is much larger than the magnitudes of the two formers. This again demonstrates that the horizontal compression loading yields a significant influence on the M-integral for the different kinds of nano-inclusion. In order to provide better understandings on the abovementioned conclusions, more detailed comparisons are needed for the second set of the surface parameters (ii). The variable tendencies of the M-integral against the loading level for the second set of surface parameters (ii) $\mu_0=-0.3760$ N/m, $\lambda_0=6.8511$ N/m, and $\sigma_0=0.9108$ N/m [17] are plotted in Figs. 3(a)–3(c). It is seen from Fig. 3(a) under the uni-axial tension loading that the four curves are similar to those shown in Fig. 2(a) for the first set of surface parameters (i). The only differences are the values of the neutral loading point, at which the M-integral transforms from a negative value to a positive value. In Fig. 3(a) the values are 120 MPa and 200 MPa for the soft inclusion and the void, respectively, much larger than 70 MPa and 90 MPa in Fig. 2(a). Under the neutral loading point, the M-integral for the soft inclusion or void is negative, representing the energy absorbing, whereas over the neutral loading point, the larger the uni-axial tension loading is, the larger the positive M-integral is, representing the energy release. Of course, the values of the M-integral in Fig. 3(a) for the rigid or hard inclusions are still always negative as those shown in Fig. 2(a), and the larger the uni-axial tension loading is, the larger the absolute value of the negative M-integral is. However, Fig. 3(b) shows a different feature from Fig. 2(b) where the M-integral for the soft inclusion is always negative without the neutral loading point (or it might be much larger than 300 MPa), whereas the neutral loading point for the void is 180 MPa, much larger than 115 MPa for the first set of surface parameters (i). Moreover, Fig. 3(c) shows the similar variable tendencies to those shown in Fig. 2(c), i.e., the neutral loading point for the two curves for the soft inclusion with symbol (□) and the void with symbol (△) is rather small: 38 MPa and 59 MPa, respectively, much smaller than 120 MPa and 200 MPa under the uni-axial tension loading. In other words, the change in the surface parameters from the first set (i) to the second set (ii) cannot influence the main variable tendencies of the M-integral against the loading level for the four kinds of inclusion with a fixed radius $R=5$ nm. It is also concluded from Fig. 3(c) that the horizontal compression loading also yield a significant influence on the M-integral, especially it significantly decreases the neutral loading point. Thus, in the most cases (Fig. 3(c)), the soft inclusion or the void nearly always yields the positive values of the M-integral with $R=5$ nm, representing the energy release rather than the energy absorbing.

Second, attention is focused on the influence of the radius for the four different kinds of nano-inclusion under the three different kinds of loading on the variable tendencies of the M-integral, especially to show more features of the M-integral analysis in nanoscale. Variable tendencies of the four different inclusions for the first set of surface parameters (i) $\mu_0=-5.4251$ N/m, $\lambda_0=3.4939$ N/m, and $\sigma_0=0.5689$ N/m are shown in Figs.

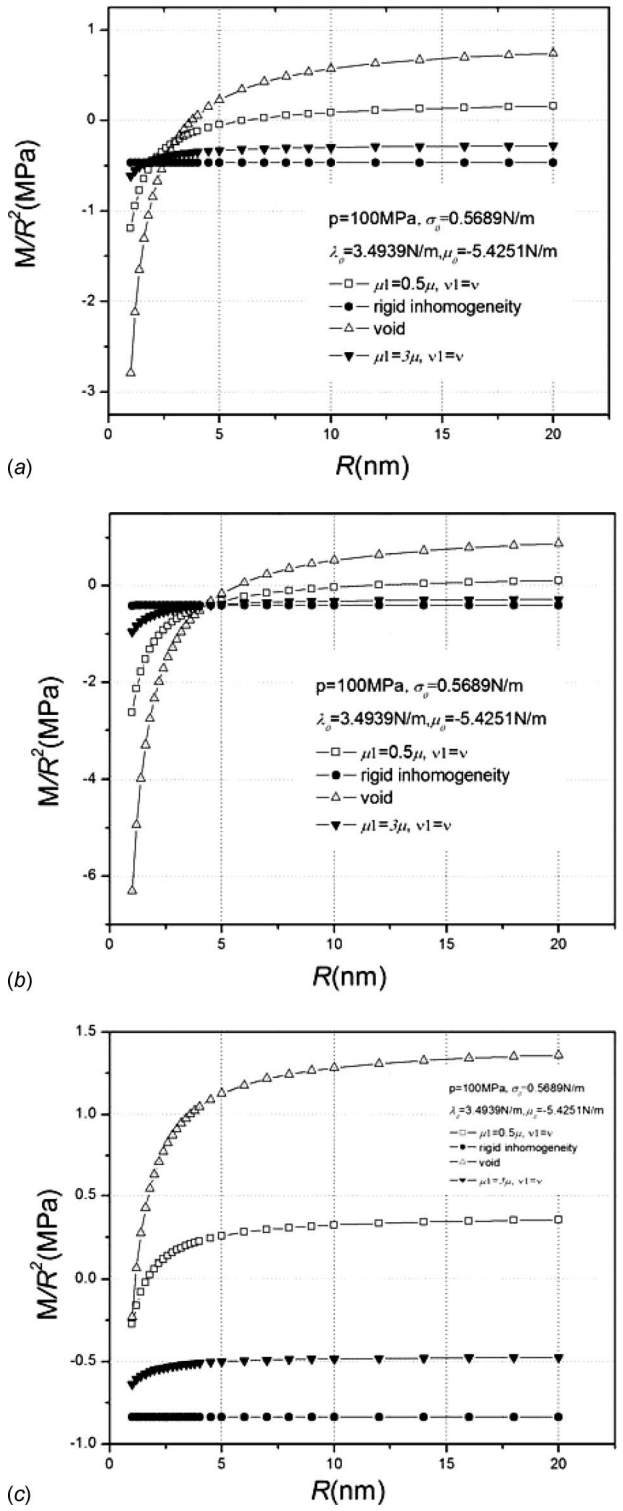

Fig. 4 The influence of inclusion radius on the *M*-integral: (*a*) uni-axial tension loading, (*b*) bi-axial tension loading, and (*c*) bi-axial tension-compression loading

4(*a*)–4(*c*) under the three kinds of loadings with $p=100$ MPa, respectively, where the radius of the different nano-inclusions varies from 1 nm to 20 nm. Of course, special attention is focused on the range of the radius between 1 nm and 5 nm, in which the size dependence of the inclusion induced from the surface parameters may become significant. On the one hand, it is not a surprise from Figs. 4(*a*)–4(*c*) that the hard inclusion with symbol (▼) and the rigid inclusion with symbol (●) always yield negative values of the *M*-integral no matter how the three different kinds of loading are chosen, and whether the radius of the inclusion is large or small. This is true because the expansion of the hard inclusion or rigid inclusion always absorbs energy rather than releases energy. It is seen from Figs. 4(*a*) and 4(*b*) that the influence of the radius for the soft inclusion with symbol (□) and the void with symbol (△) on the *M*-integral is very small when the radius is larger than 10 nm but the influence becomes significant when the radius is much less than 10 nm. That is, the *M*-integral divided by R^2 (for seeing more clearly) decreases significantly for the soft inclusion and the void as the radius of the inclusion decreases from 10 nm to 1 nm, especially in the range between 1 nm and 5 nm. On the other hand, there is little influence of the radius for the rigid inclusion on the *M*-integral even though the radius is very small, e.g., within the range between 1 nm and 5 nm, whereas the influence of the radius for the hard inclusion on the *M*-integral is very small except the cases when the radius is less than 2.5 nm. However, for the void, the uni-axial tension loading and the bi-axial tension loading yield quite different features of the variable tendencies of the *M*-integral within the range of the radius between 1 nm and 5 nm. It is seen from Fig. 4(*a*) that under the uni-axial tension loading $p=100$ MPa the *M*-integral for the soft inclusion or void within the range between 1 nm and 5 nm can be either positive or negative; whereas in Fig. 4(*b*) under the bi-axial tension loading it is always negative for the void within the range between 1 nm and 5 nm. Of great interest are the variable tendencies of the *M*-integral under the bi-axial tension-compression loading as shown in Fig. 4(*c*). It is seen that the horizontal compression loading yields significant influence on the variable tendencies of the *M*-integral as compared with those under uni-axial or bi-axial tension loading shown in Figs. 4(*a*) and 4(*b*). That is, unlike those shown in Figs. 4(*a*) and 4(*b*) where the four curves corresponding to the four kinds of inclusion are always intersected, the derivations among the four curves corresponding to the soft inclusion, the rigid inclusion, the void, and the hard inclusion, under the bi-axial tension-compression loading, are remarkable without any intersecting as shown in Fig. 4(*c*). This finding is significant, which has not reported in the literature. Moreover, in the most cases within the range between 1 nm and 5 nm in Fig. 4(*c*), the *M*-integral for the soft inclusion or void is positive, representing the energy release due to the expansion of the soft inclusion or void. Although the hard inclusion and the rigid inclusion still yield negative values of the *M*-integral, which are less influenced by the radius, in the most cases, the soft inclusion and void always yield positive values of the *M*-integral under $p=100$ MPa even though the radius is 1.2 nm. Particularly, the derivations between the two curves corresponding to the soft inclusion and the void are of significance. For example, for $R=5$ nm, the value of M/R^2 for the void is 1.25 MPa, whereas the value for the soft inclusion is merely 0.25 MPa, i.e., five times smaller than the former; for $R=2.5$ nm, the value of M/R^2 for the void is 0.70 MPa, whereas the value for the soft inclusion is merely 0.12 MPa, i.e., about six times smaller than the former. In fact, the derivations between the two curves corresponding to the hard inclusion and the rigid inclusion are also remarkable due to the existence of the horizontal compression loading but this observation is worthless or not important.

Third, for comparison, numerical results for the second set of surface parameters (ii) $\mu_0=-0.3760$ N/m, $\lambda_0=6.8511$ N/m, and $\sigma_0=0.9108$ N/m are plotted in Figs. 5(*a*)–5(*c*) under the three kinds of loadings with $p=30$ MPa, respectively. Quite the contrary, it is seen that the variable tendencies of the *M*-integral against the radius are significantly different from those for the first set of surface parameter (i) as compared with those shown in Figs. 4(*a*)–4(*c*). For example, in every case in Figs. 5(*a*) and 5(*b*), the value of the *M*-integral is always negative no matter how large the radius is chosen and whatever which kind of inclusion it is. It is also seen from Fig. 5(*c*) that, unlike those in Fig. 4(*c*), there are

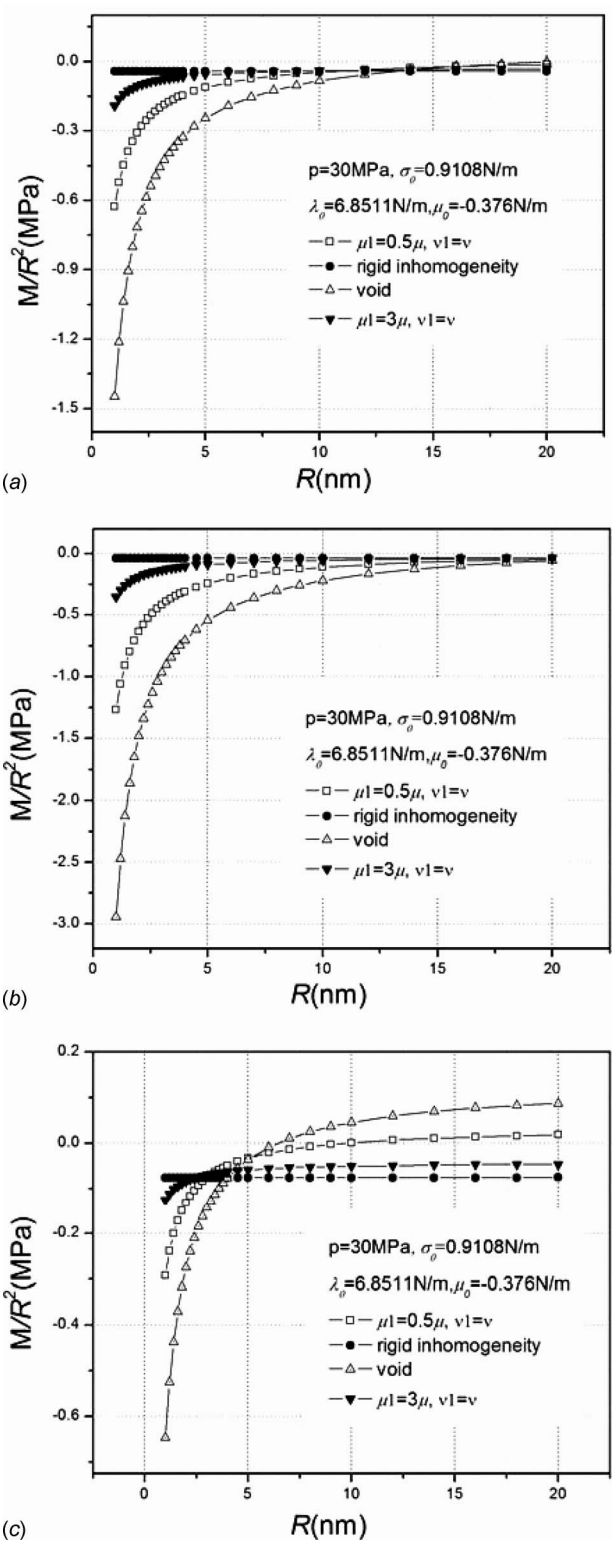

Fig. 5 The influence of inclusion radius on the *M* integral: (a) uni-axial tension loading, (b) bi-axial tension loading, and (c) bi-axial tension-compression loading

several intersecting points for the four curves under the bi-axial tension-compression loading. It is concluded that the second set (ii) with $\mu_0=-0.3760$ N/m, $\lambda_0=6.8511$ N/m, and $\sigma_0=0.9108$ N/m yields quite different influences on the variable tendencies of the M-integral against the inclusion radius from those induced from the first set (i) with $\mu_0=-5.4251$ N/m, $\lambda_0=3.4939$ N/m, and $\sigma_0=0.5689$ N/m.

Finally, it is noticed that there are two questions for the M-integral analysis in nanodefect mechanics remaining to be clarified, which are not found in macro-/microscale. The first is why or how the M-integral could be negative for the soft inclusion or void representing the energy absorbing? The second is that which parameter among the three surface parameters μ_0, λ_0, and σ_0 is the dominant one, yielding the main influence on the M-integral when the radius of inclusion is in nanoscale?

These two questions will be clarified in the sequel.

5 Conclusions and Remarks

From the analyses and discussions performed above, the following conclusions and remarks could be summarized.

(1) Unlike in macro-/microscale, the M-integral for a nanohole or a nanosoft inclusion could be either positive or negative depending on the remote tensile loading level. Moreover, there is a neutral loading point, at which a transformation from a negative value to a positive value of the M-integral occurs.

(2) It is found that due to the existence of the surface tension and the surface elasticity, the expansion of the nanohole or nanosoft inclusion under a relatively lower tensile loading absorbs the energy rather than releases the energy.

(3) It is concluded that for a nanovoid or soft inclusion under bi-axial loading, the horizontal tensile loading increases the neutral loading point, whereas the horizontal compression loading decreases the neutral loading point.

(4) In nanoscale from 1 nm to 20 nm the surface tension and surface elasticity (i.e., the three parameters) for a hard inclusion (or rigid inclusion) have little influence on the M-integral, and the values of the M-integral are always negative as they would be in macro-/microscale. Thus, from the energy release/absorbing view point, the influence of the surface tension and surface elasticity for the hard inclusion or rigid inclusion could be neglected.

(5) Detailed comparisons between the numerical results for the first set of parameters (i) $\mu_0=-5.4251$ N/m, $\lambda_0=3.4939$ N/m, and $\sigma_0=0.5689$ N/m and those for the second set of parameters (ii) $\mu_0=-0.3760$ N/m, $\lambda_0=6.8511$ N/m, and $\sigma_0=0.9108$ N/m [17] reveal that the second set (ii) leads to a much larger influence on the M-integral than the first set (i). In other words, for a nanohole or a nanosoft inclusion the second set (ii) yields much larger energy absorbing (when the M-integral is negative) or energy release (when the M-integral is positive).

Acknowledgment

This work was supported by the NSFC of Grant No. 10872154 and the Doctor foundation of the Chinese Education Ministry. Also, the Humboldt foundation of Germany for Y.-H.C. and the host Professor U. Gabbert are greatly appreciated.

References

[1] Ortiz, M., 1999, "Nanomechanics of Defects in Solids," Adv. Appl. Mech., **36**, pp. 2–79.
[2] Kuzumaki, T., Miyazawa, K., Ichinose, H., and Ito, K., 1998, "Processing of Carbon Nanotube Reinforced Aluminum Composite," J. Mater. Res., **13**, pp. 2445–2449.
[3] Cui, Y., and Lieber, C. M., 2001, "Functional Nanoscale Electronic Devices Assembled Using Silicon Nanowire Building Blocks," Science, **291**, pp. 851–853.
[4] Miller, R. E., and Shenoy, V. B., 2000, "Size-Dependent Elastic Properties of Nanosized Structural Elements," Nanotechnology, **11**, pp. 139–147.
[5] Shenoy, V. B., 2002, "Size-Dependent Rigidities of Nanosized Torsional Elements," Int. J. Solids Struct., **39**, pp. 4039–4052.
[6] Gibbs, J. W., 1906, *Scientific Papers*, Vol. 1, Longmans-Green, London.
[7] Nix, W. D., and Gao, H., 1998, "An Atomistic Interpretation of Interface

Stress," Scr. Mater., **39**, pp. 1653–1661.
[8] Gurtin, M. E., and Murdoch, A. I., 1975, "A Continuum Theory of Elastic Material Surfaces," Arch. Ration. Mech. Anal., **57**, pp. 291–323.
[9] Gurtin, M. E., Weissmuller, J., and Larché, F., 1988, "A General Theory of Curved Deformable Interfaces in Solids at Equilibrium," Philos. Mag. A, **78**, pp. 1093–1109.
[10] Sharma, P., and Ganti, S., 2002, "Interfacial Elasticity Corrections to Size-Dependent Strain-State of Embedded Quantum Dots," Phys. Status Solidi B, **234**, pp. R10–R12.
[11] Sharma, P., and Ganti, S., 2004, "Size-Dependent Eshelby's Tensor for Embedded Nano-Inclusions Incorporating Surface/Interface Energies," ASME J. Appl. Mech., **71**, pp. 663–671.
[12] Sharma, P., and Wheeler, L. T., 2007, "Size-Dependent Elastic State of Ellipsoidal Nano-Inclusions Incorporating Surface/Interface Tension," ASME J. Appl. Mech., **74**, pp. 447–455.
[13] Sharma, P., Ganti, S., and Bhate, N., 2003, "Effect of Surfaces on the Size-Dependent Elastic State of Nano-Inhomogeneities," Appl. Phys. Lett., **82**, pp. 535–537.
[14] Duan, H. L., Wang, J., Huang, Z. P., and Luo, Z. Y., 2005, "Stress Concentration Tensors of Inhomogeneities With Interface Effects," Mech. Mater., **37**, pp. 723–736.
[15] Duan, H. L., Wang, J., Huang, Z. P., and Karihaloo, B. L., 2005, "Eshelby Formalism for Nano-Inhomogeneities," Proc. R. Soc. London, Ser. A, **461**, pp. 3335–3353.
[16] Lim, C. W., Li, Z. R., and He, L. H., 2006, "Size-Dependent, Non-Uniform Elastic Field Inside a Nano-Scale Spherical Inclusion Due to Interface Stress," Int. J. Solids Struct., **43**, pp. 5055–5065.
[17] Tian, L., and Rajapakse, R. K. N. D., 2007, "Analytical Solution for Size-Dependent Elastic Field of a Nanoscale Circular Inhomogeneity," ASME J. Appl. Mech., **74**, pp. 568–574.
[18] Mogilevskaya, S. G., Crouch, S. L., and Stolarski, H. K., 2008, "Multiple Interacting Circular Nano-Inhomogeneities With Surface/Interface Effects," J. Mech. Phys. Solids, **56**, pp. 2298–2327.
[19] Wang, G. F., and Wang, T. J., 2006, "Surface Effects on the Diffraction of Plane Compressional Waves by a Nanosized Circular Hole," Appl. Phys. Lett., **89**, p. 231923.
[20] Yang, F. Q., 2004, "Size-Dependent Effective Modulus of Elastic Composite Materials: Spherical Nanocavities at Dilute Concentrations," J. Appl. Phys., **95**, pp. 3516–3520.
[21] Duan, H. L., Wang, J., Huang, Z. P., and Karihaloo, B. L., 2005, "Size-Dependent Effective Elastic Constants of Solids Containing Nano-inhomogeneities With Interface Stress," J. Mech. Phys. Solids, **53**, pp. 1574–1596.
[22] Marian, J., Knap, J., and Ortiz, M., 2005, "Nanovoid Deformation in Aluminum Under Simple Shear," Acta Mater., **53**, pp. 2893–2900.
[23] Borodich, F. M., and Keer, L. M., 2004, "Evaluation of Elastic Modulus of Materials by Adhesive (No-Slip) Nano-Indentation," Proc. R. Soc. London, Ser. A, **460**, pp. 507–514.
[24] Hu, N., Fukunaga, H., Lu, C., Kameyama, M., and Yan, B., 2003, "Prediction of Elastic Properties of Carbon Nanotube Reinforced Composites," Proc. R. Soc. London, Ser. A, **461**, pp. 1685–1710.
[25] Lloyd, S. J., Castellero, A., Giuliani, F., Long, Y., McLaughlin, K. K., Molina-Aldareguia, J. M., Stelmashenko, N. A., Vandeperre, L. J., and Clegg, W. J., 2003, "Observations of Nanoindents Via Cross-Sectional Transmission Electron Microscopy: A Survey of Deformation Mechanisms," Proc. R. Soc. London, Ser. A, **461**, pp. 2521–2543.
[26] Jayaweera, N. B., Downes, J. R., Frogley, M. D., Hopkinson, M., Bushby, A. J., Kidd, P., Kelly, A., and Dunstan, D. J., 2003, "The Onset of Plasticity in Nanoscale Contact Loading," Proc. R. Soc. London, Ser. A, **459**, pp. 2049–2068.
[27] Garg, A., Han, J., and Sinnott, S. B., 1998, "Interactions of Carbon-Nanotube Proximal Probe Tips With Diamond and Graphene," Phys. Rev. Lett., **81**, pp. 2260–3.
[28] Poncharal, P., Wang, Z., Ugarte, D., and deHeer, W. A., 1999, "Electrostatic Deflections and Electromechanical Resonances of Carbon Nanotubes," Science, **283**, pp. 1513–1516.
[29] Terrones, M., Grobert, N., Hsu, W., Zhu, Y., Hu, W., Terrones, H., Hare, J., Kroto, H., and Walton, D., 1999, "Advances in the Creation of Filled Nanotubes and Novel Nanowires," MRS Bull., **24**, pp. 43–49.
[30] Wong, E., Sheehan, P. E., and Lieber, C. M., 1997, "Nanobeam Mechanics: Elasticity, Strength, and Toughness of Nanorods and Nanotubes," Science, **277**, pp. 1971–1975.
[31] Yakobson, B. I., 1998, "Mechanical Relaxation and 'Intramolecular Plasticity' in Carbon Nanotubes," Appl. Phys. Lett., **72**, pp. 918–920.
[32] Yakobson, B. I., Brabec, C. J., and Bernhole, J., 1996, "Nanomechanics of Carbon Tubes: Instabilities Beyond Linear Response," Phys. Rev. Lett., **76**, pp. 2511–2514.
[33] Sharma, P., and Ganti, S., 2005, "Erratum: "Size-Dependent Eshelby's Tensor for Embedded Nano-Inclusions Incorporating Surface/Interface Energies" [Journal of Applied Mechanics, 2004, 71(5), pp. 663–671]," ASME J. Appl. Mech., **72**, p. 628.
[34] Dingreville, R., Qu, J., and Cherkauoi, M., 2005, "Surface Free Energy and Its Effect on the Elastic Behavior of Nano-Sized Particles, Wires and Films," J. Mech. Phys. Solids, **53**, pp. 1827–1854.
[35] Park, H. S., and Klein, P. A., 2008, "Surface Stress Effects on the Resonant Properties of Metal Nanowires: The Importance of Finite Deformation Kinematics and the Impact of the Residual Surface Stress," J. Mech. Phys. Solids, **56**, pp. 3144–3166.
[36] Knowles, J. K., and Sternberg, E., 1972, "On a Class of Conservation Laws in Linearized and Finite Elastostatics," Arch. Ration. Mech. Anal., **44**, pp. 187–211.
[37] Budiansky, B., and Rice, J. R., 1973, "Conservation Laws and Energy-Release Rates," ASME J. Appl. Mech., **40**, pp. 201–203.
[38] Eshelby, J. D., 1974, "Calculation of Energy Release Rate," *Prospects of Fracture Mechanics*, G. C. Sih and D. Broek, eds., Noordhoff International, Groningen, The Netherlands, pp. 69–84.
[39] Freund, L. B., 1978, "Stress-Intensity Factor Calculations Based on a Conservation Integral," Int. J. Solids Struct., **14**, pp. 241–250.
[40] Herrmann, A. G., and Herrmann, G., 1981, "On Energy Release Rates for a Plane Crack," ASME J. Appl. Mech., **48**, pp. 525–528.
[41] Eischen, J. W., and Herrmann, G., 1987, "Energy Release Rates and Related Balance Laws in Linear Elastic Defect Mechanics," ASME J. Appl. Mech., **54**, pp. 388–392.
[42] Choi, N. Y., and Earmme, Y. Y., 1992, "Evaluation of Stress Intensity Factors in Circular Arc-Shaped Interfacial Crack Using *L* Integral," Mech. Mater., **14**, pp. 141–153.
[43] Seed, G. M., 1997, "The Boussinesq Wedge and the J_k, *L*, and *M* Integrals," Fatigue Fract. Eng. Mater. Struct., **20**, pp. 907–916.
[44] Chen, Y. H., 2001, "*M*-Integral for Two Dimension Solids With Strongly Interacting Cracks. Part I: In an Infinite Brittle Solids," Int. J. Solids Struct., **38**, pp. 3193–3212.
[45] Chen, Y. H., 2001, "*M*-Integral for Two-Dimensional Solids With Strongly Interacting Cracks. Part II: In the Brittle Phase of an Infinite Metal/Ceramic Biomaterial," Int. J. Solids Struct., **38**, pp. 3213–3232.
[46] Li, Q., and Chen, Y. H., 2008, "Surface Effect and Size Dependent on the Energy Release Due to a Nanosized Hole Expansion in Plane Elastic Materials," ASME J. Appl. Mech., **75**, p. 061008.